

ORIGINAL RESEARCH

 OPEN ACCESS

Recognition and killing of cancer stem-like cell population in hepatocellular carcinoma cells by cytokine-induced killer cells via NKG2d-ligands recognition

Xiao-Xiang Rong^{a,b,*}, Fang Wei^{c,*}, Xiao-Lin Lin^{c,*}, Yu-Juan Qin^c, Lin Chen^c, Hui-Yan Wang^c, Hong-Fen Shen^c, Li-Ting Jia^d, Rao-Ying Xie^c, Tao-Yan Lin^c, Wei-Chao Hao^c, Jie Yang^c, Sheng Yang^c, Yu-Shuang Cheng^c, Wen-Hua Huang^e, Ai-min Li^a, Yan Sun^f, Rong-Cheng Luo^a, and Dong Xiao^{c,g}

^aDepartment of Oncology, Traditional Chinese Medicine-Integrated Hospital, Southern Medical University, Guangzhou, China; ^bDepartment of Oncology, Nanfang Hospital, Southern Medical University, Guangzhou, China; ^cGuangdong Provincial Key Laboratory of Cancer Immunotherapy and Guangzhou Key Laboratory of Tumor Immunology Research, Cancer Research Institute, Southern Medical University, Guangzhou, China; ^dDepartment of Pathology, Guilin Medical College, Guilin, China; ^eDepartment of Anatomy, Guangdong Provincial Key Laboratory of Construction and Detection in Tissue Engineering, School of Basic Medical Science, Southern Medical University, Guangzhou, China; ^fChildren's Hospital Boston, Harvard Medical School, Boston, MA, USA; ^gInstitute of Comparative Medicine & Laboratory Animal Center, Southern Medical University, Guangzhou, China

ABSTRACT

There is an urgent need for more potent and safer approaches to eradicate cancer stem cells (CSCs) for curing cancer. In this study, we investigate cancer-killing activity (CKA) of cytokine-induced killer (CIK) cells against CSCs of hepatocellular carcinoma (HCC). To visualize CSCs *in vitro* by fluorescence imaging, and image and quantify CSCs in tumor xenograft-bearing mice by bioluminescence imaging, HCC cells were engineered with CSC detector vector encoding GFP and luciferase controlled by Nanog promoter. We found that CIK cells have a strong CKA *in vitro* against putative CSCs of HCC, as shown by tumorsphere formation and time-lapse imaging. Additionally, time-lapse recording firstly revealed that putative CSCs were attacked simultaneously by many CIK cells and finally eradicated by CIK cells, indicating the necessity of achieving sufficient effector-to-target ratios. We firstly illustrated that anti-NKG2D antibody blocking partially but significantly inhibited CKA of CIK cells against putative CSCs. More importantly, intravenous infusion of CIK cells remarkably delayed tumor growth in mice with a significant decrease in putative CSC number monitored by bioluminescence imaging. Taken together, these findings demonstrate CKA of CIK cells against putative CSCs of HCC, at least in part, by NKG2D-ligands recognition.

Abbreviations: BsAb, bispecific antibodies; CARs, chimeric antigen receptors; CIK cells, Cytokine-induced killer cells; CKA, cancer-killing activity; CSCs, cancer stem cells; DFS, disease-free survival; FACS, Fluorescence activated cell-sorting; HCC, hepatocellular carcinoma; MHC, major histocompatibility complex; OS, overall survival; PBMcs, Peripheral blood mononuclear cells; RFA, radiofrequency ablation; TACE, transarterial chemoembolization; TICs, tumor-initiating cells.

ARTICLE HISTORY

Received 29 July 2015
Revised 16 August 2015
Accepted 19 August 2015

KEYWORDS

Cancer stem cells; cytokine-induced killer cells; hepatocellular carcinoma; *in vivo* bioluminescence imaging; NKG2D-ligands recognition; promoter-reporter gene strategy; time-lapse recording

Introduction




HCC causes a high mortality rate in many counties.¹ Patients with HCC usually have a poor prognosis. Despite various treatments including surgery, radiofrequency ablation (RFA) and transarterial chemoembolization (TACE) have been performed for HCC, the overall 5-y survival rate of HCC patients has remained relatively low due to the high recurrence rates.²⁻³ Therefore, novel and effective therapy for HCC is urgently warranted.


The development of immunotherapy for HCC treatment has received considerable attention.⁴⁻⁵ CIK cells are *ex vivo* expanded T natural killer (NK) lymphocytes characterized by the

co-expression of CD3 and CD56 molecules.⁶⁻⁷ The strong antitumor activity and the absence of specific major histocompatibility complex (MHC) restrictions are crucial characteristics that favors CIK cells over conventional cytotoxic T lymphocytes.⁶⁻¹⁰

In the field of HCC, CIK cells infusion, as an adjuvant therapy, can reduce the recurrence rate, and prolong the disease-free survival (DFS) and overall survival (OS).^{5,11-13} More importantly, minimal toxicity was observed in these pretreated patients. However, intensive research work still needs to be done to improve CIK cell-based cancer therapy.⁶⁻⁷

CSCs/tumor-initiating cells (TICs), which are responsible for initiating and maintaining cancer, and contribute to

CONTACT Dong Xiao  Xiao_d@hotmail.com; Rong-Cheng Luo  luorc01@163.com; Yan Sun  suny528@gmail.com

 Supplemental data for this article can be accessed on the publisher's website.

*These authors contributed equally to this work.

Published with license by Taylor & Francis Group, LLC © Xiao-Xiang Rong, Fang Wei, Xiao-Lin Lin, Yu-Juan Qin, Lin Chen, Hui-Yan Wang, Hong-Fen Shen, Li-Ting Jia, Rao-Ying Xie, Tao-Yan Lin, Wei-Chao Hao, Jie Yang, Sheng Yang, Yu-Shuang Chen, Wen-Hua Huang, Ai-min Li, Yan Sun, Rong-Cheng Luo, and Dong Xiao
This is an Open Access article distributed under the terms of the Creative Commons Attribution-Non-Commercial License (<http://creativecommons.org/licenses/by-nc/3.0/>), which permits unrestricted non-commercial use, distribution, and reproduction in any medium, provided the original work is properly cited. The moral rights of the named author(s) have been asserted.

cancer recurrence, metastasis and therapeutic resistance, are the root cause for cancer treatment failure.¹⁴⁻²² Consequently, one of the key goals in cancer research has been to develop therapeutic strategies to efficiently and safely eradicate CSC population for curing cancer, while one of the major advantages of most immunotherapeutic strategies is low or acceptable toxicity.²³

Patient-derived CIK cells killed putative CSCs of autologous metastatic melanoma,²⁴ and autologous metastatic bone sarcoma and soft-tissue sarcomas,²⁵ which will be still required to be verified by further evidence (i.e., tumor sphere formation, time-lapse imaging, *in vivo* experiment, etc.) and in various cancers. Furthermore, up to now, the antitumor killing activity of CIK cells against CSCs of HCC is completely unexplored. In this study, we fully investigated the effects of CIK cell treatment on stem cell-like populations in HCC as well as the underlying mechanisms by using various approaches.

Results

CIK cell treatment significantly decreased the stem cell-like population in HCC

CIK cells were successfully expanded from fresh peripheral blood mononuclear cells (PBMCs) with the timed addition of IFN γ , immobilized anti-CD3 antibodies and IL-2. Flow cytometric analysis of CIK cell phenotype was shown in “Supplemental Results” section and Fig. S1. Since our data from “Supplemental Results” section demonstrated that CIK cells illustrated a strong antitumor activity *in vitro* against HCC cells

(Fig. 1), we further determine the effects of CIK cell treatment on stem cell-like populations in HCC.

A tumorsphere is a solid, spherical formation developed from the proliferation of one cancer stem/progenitor cells, and only cancer stem/progenitor cells can survive and proliferate in serum-free, non-adherent conditions to form tumor spheres.³¹⁻³⁴ Thus, by tumor sphere formation assay, we examined the ability of SMMC7721 and Huh7 cells to form tumor spheres after treated with CIK cells at different E:T ratios. The results showed that CIK-treated SMMC7721 and Huh7 target cells demonstrated a dramatical reduction in the number of tumor spheres formed in a dose-dependent manner (Fig. 2A,B). Furthermore, tumor spheres were efficiently scavenged by CIK cells when tumor spheres formed from SMMC7721 cells were co-cultured with CIK cells for one day (Fig. 2C). Together, our results indicate that heterogeneous CIK cell populations have a strong cancer killing activity (CKA) *in vitro* against putative CSCs within a population of *in vitro* cultured HCC cells.

Visualization of putative CSCs of HCC with a “CSC detector”

The commonly used optical molecular imaging techniques include fluorescence imaging and bioluminescence imaging which have their own advantages.³⁵⁻³⁷ Nanog has been frequently served as CSC-related markers to identify putative CSC population from clinical samples and cell lines in various cancers, including HCC.³⁸ Hence, based on promoter-reporter gene strategy, we have devised and constructed the lentivirus vector of pLV-P_{Nanog}-GFP-T2A-Luc harboring GFP and Luc under control of human Nanog promoter (Fig. 3A), which

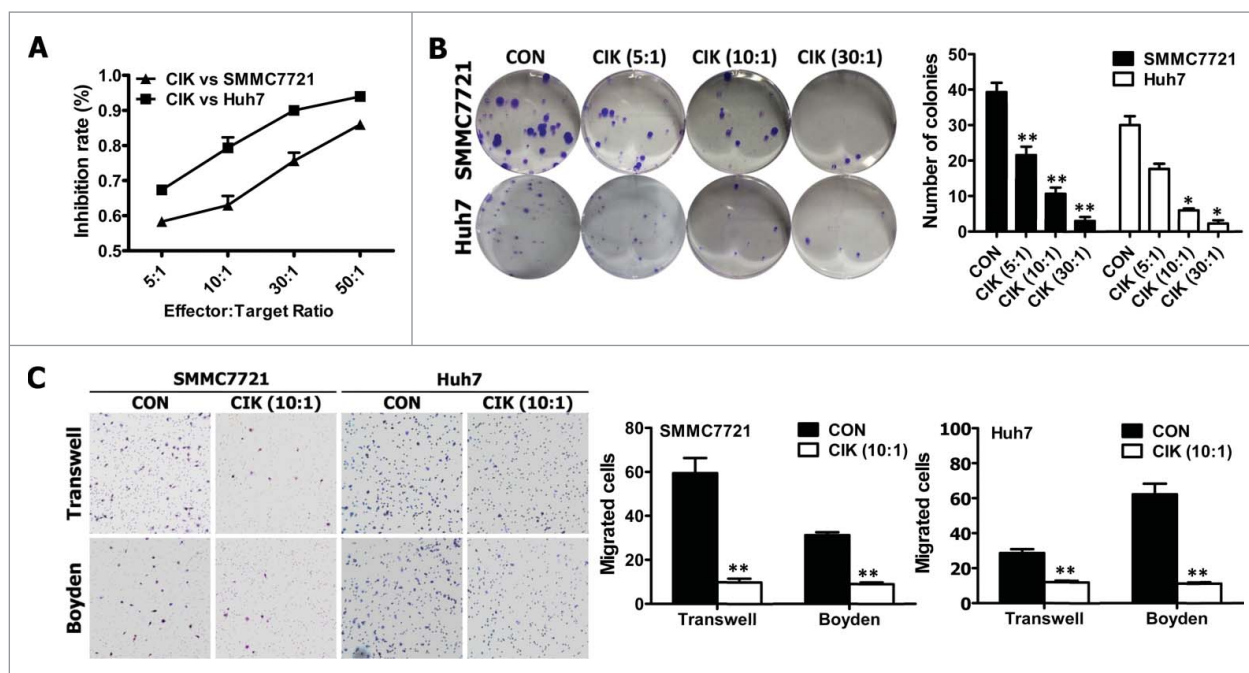


Figure 1. CIK cells efficiently killed HCC cells *in vitro*. CIK cells were successfully expanded from fresh PBMCs with the timed addition of IFN γ , immobilized anti-CD3 antibodies and IL-2. (A) Colony formation assay for CIK-treated SMMC7721 and Huh7 cells. (B) The proliferation ability of SMMC7721 and Huh7 cells treated with CIK cells were analyzed by CCK8 assay. (C) CIK-treated HCC cells exhibited less motile and invasive ability. The motility and invasion of SMMC7721 and Huh7 cells were analyzed with an *in vitro* migration assay using a transwell chamber and an *in vitro* invasion assay using a matrigel-coated Boyden chamber, respectively. The migrated cells were plotted as the average number of cells per field of view from three different experiments, as described in the materials and methods section. Error bars represent as mean \pm SD (* p < 0.05, ** p < 0.01 compared to controls without CIK cell treatment).

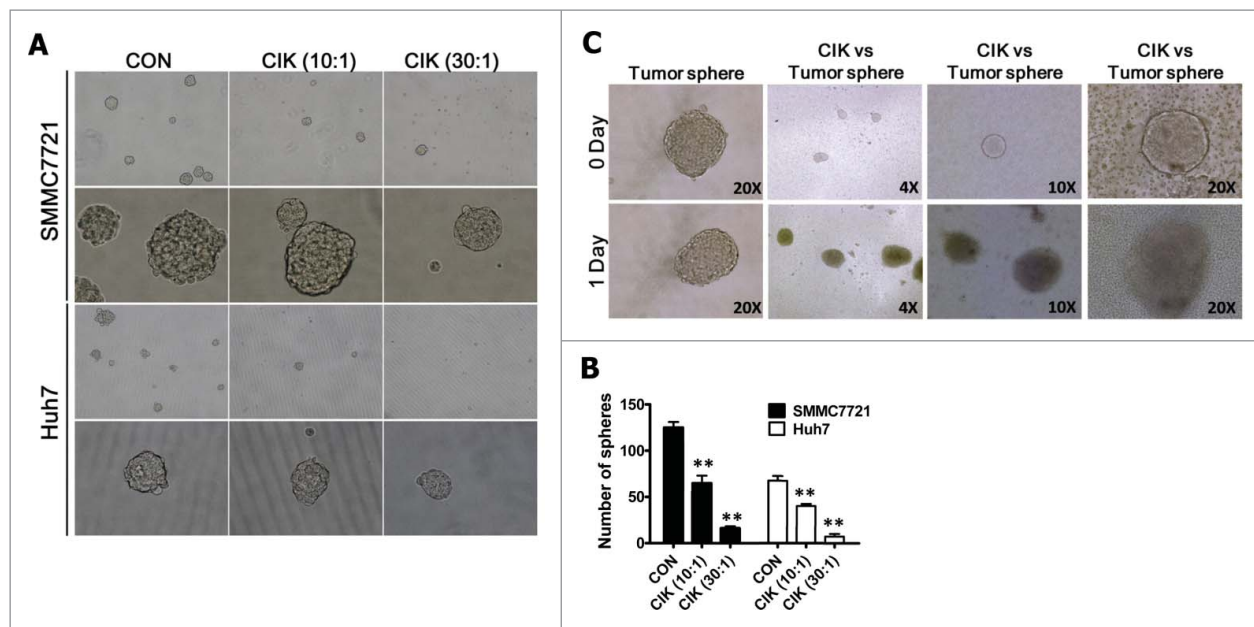


Figure 2. CIK cells efficiently killed stem-like cancer cells of HCC *in vitro*. (A–B) Images showing tumor sphere formation in CIK-treated SMMC7721 and Huh7 cells. Sphere size and density are shown in the left panels (A), and the number of spheres is shown in the right panels (B). (C) CIK cells efficiently killed tumor spheres derived from SMMC7721 cells. Error bars represent as mean \pm SD (* $p < 0.05$, ** $p < 0.01$ compared to controls without CIK cell treatment).

allows us to take advantage of fluorescence and bioluminescence imaging to visualize putative CSCs within *in vitro* cultured cancer cells and *in vivo* optically image and quantify a rare population of putative CSCs in human tumor xenograft-bearing mice.

To optically visualize putative CSCs, SMMC7721 and Huh7 cells were infected with lentiviruses carrying P_{Nanog} -GFP-T2A-Luc transgene (Fig. 3A). Ten days after infection, we observed that GFP was highly expressed in a small percentage of stably infected HCC cells (Fig. 3B). Fluorescence activated cell-sorting (FACS) analysis revealed the average GFP expression was 5.3% in SMMC7721 cells and 3.9% in Huh7 cells (Fig. 3C). Importantly, Luc signal (max photons/sec/cm²/sr) correlated strongly with SMMC7721 cell numbers ($r^2 = 0.996$) (Fig. 3D,E).

Next, GFP-positive (GFP+) and GFP-negative (GFP-) cells were sorted, and then gene expression was analyzed and the respective assays mentioned below were performed (Fig. 3F–I). As shown in Fig. 3F, in comparison with GFP- cells, the significantly increased expression of stem cell markers Nanog, Oct4 and Sox2 was found in sorted GFP+ SMMC7721 and Huh7 cells, suggesting that GFP+ cells might have stem-cell-like characteristics.

CSCs can form tumorspheres *in vitro* in a non-attached culture condition.^{32,38} As shown in Fig. 3G, GFP+ cells formed more spheres than GFP- cells did in SMMC7721 cells. Moreover, approximately 26.6% GFP+ cells (for SMMC7721) and 15.7% (for Huh7) GFP+ cells can form spheres and all spheres exhibited GFP expression (Fig. 3G). Additionally, colony formation assay indicated that GFP+ cells were able to induce more colonies than GFP- cells (Fig. 3H). Collectively, GFP+ cancer cells exhibit the characteristics of CSCs.

In addition, our data exhibited that GFP+ cells showed 17.4 folds increase in motile capacity, and 8.1 times increase in invasive ability, respectively, compared with GFP- cells (Fig. 3I).

Our data demonstrated that GFP+ cancer cells harboring P_{Nanog} -GFP-T2A-Luc transgene exhibit the characteristics of CSCs. Thus, the newly established SMMC7721 cells harboring P_{Nanog} -GFP-T2A-Luc transgene allows us to *in vitro* visualize putative CSCs by fluorescence imaging and *in vivo* optically image and quantify putative CSCs in human tumor xenograft-bearing mice by bioluminescence imaging.

Tumor-killing activity of CIK cells remained equally effective against both putative CSCs and non-CSCs of HCC

Based on GFP expression, HCC cells harboring P_{Nanog} -GFP-T2A-Luc transgene were sorted into two fractions (GFP+ and GFP-) that served as targets to assess separately the antitumor activity of CIK cells against GFP+ (putative CSCs) and GFP- cells. Our results showed that the tumor-killing activity of CIK cells remained equally effective against both GFP+ and GFP- HCC cells (Fig. 4A).

Time-lapse imaging revealed the direct killing effect of CIK cells on stem-like cancer cells of HCC

To optically visualize the killing process of CIK cells against cancer cells, putative CSCs or tumor spheres, we performed time-lapse video recording (Fig. 4B,C,E, and Movies S1–3). First, we visualized the killing process of CIK cells against SMMC7721 cells by time-lapse imaging, and observed that one cancer cell was usually attacked simultaneously by many CIK cells and finally killed by CIK cells (Fig. 4B and Movie S1).

Secondly, we used time-lapse video recording to visualize the killing process of CIK cells against putative CSCs and non-CSCs of HCC (Fig. 4C and Movie S2). Time-lapse fluorescence video fully revealed that the antitumor activity of CIK cells was equally intense against both GFP+ and GFP- cancer cells (Fig. 4C and Movie S2), and that each of

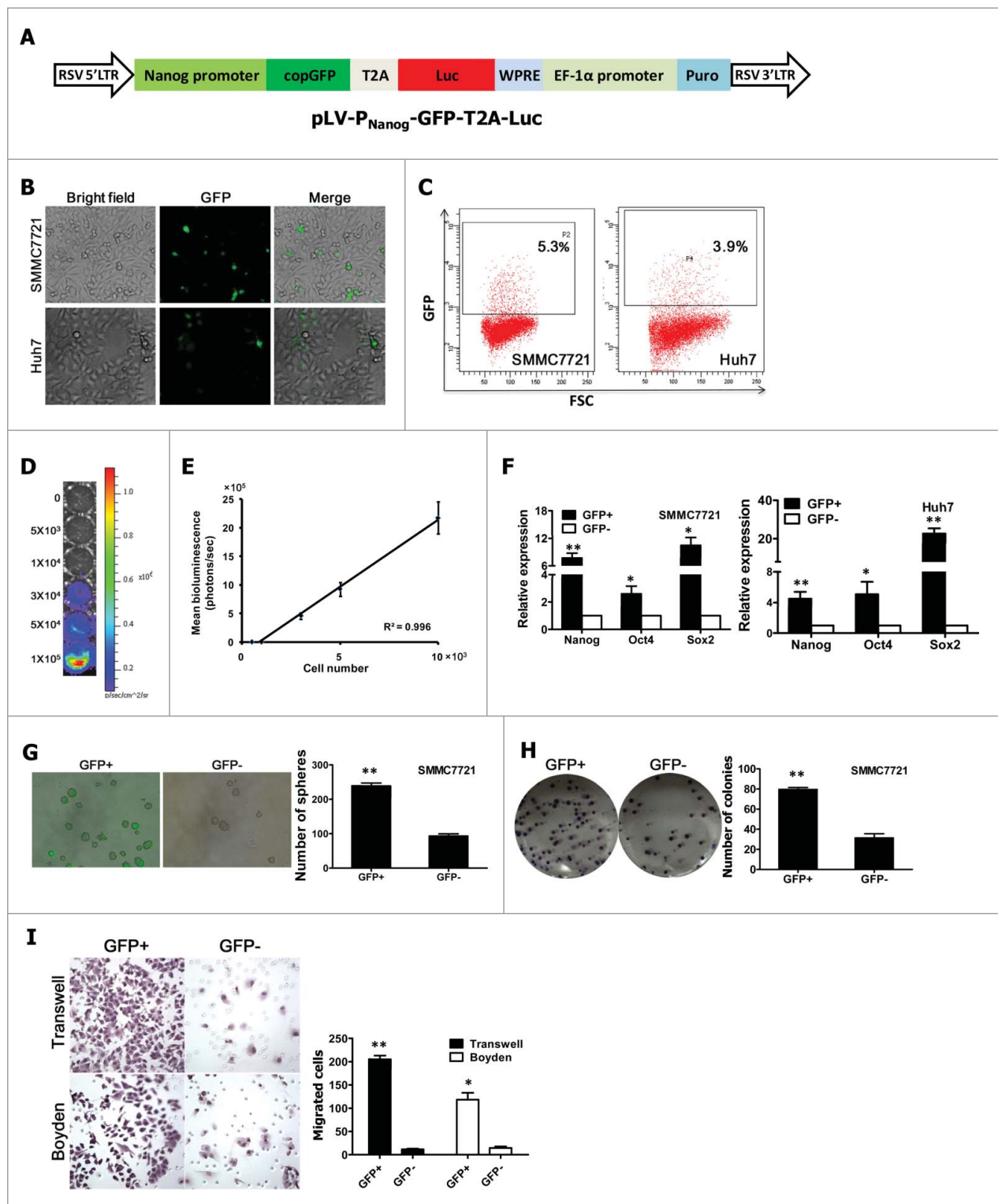


Figure 3. Visualization of stem-like cancer cells of HCC with a "CSC detector." (A) Schematic representation of lentiviral vector pLV-P_{Nanog}-GFP-T2A-Luc used to visualize stem-like cancer cells. The construct map is not drawn to the scale. Abbreviations: Luc: firefly luciferase; GFP: green fluorescent protein. (B–C) Representative GFP expression was measured in HCC cell lines (e.g., SMMC7721 and Huh7) carrying P_{Nanog}-GFP-T2A-Luc transgene by inverted fluorescence microscope (B) and by flow cytometry (C). (D) SMMC7721 cells harboring Luc have robust reporter gene expression as shown by bioluminescence imaging (BLI). (E) A strong correlation exists between BLI signal and SMMC7721 cell number. (F–G) GFP⁺ and GFP⁻ fractions sorted from SMMC7721 and Huh7 cells carrying P_{Nanog}-GFP-T2A-Luc transgene (shown in Fig. 3B,C) by fluorescence-activated cell sorting (FACS) were subjected to RT-PCR for the detection of stem cell markers (e.g., Nanog, Oct4, and Sox2) (F), and tumor spheroid formation assay (G). (H–I) The growth (H), migration (I) and invasion (I) of GFP⁺ and GFP⁻ HCC cells were evaluated by colony formation assay, transwell migration assay and matrigel-coated Boyden chamber assay, respectively. GFP⁺ and GFP⁻ fractions were sorted from SMMC7721 and Huh7 cells carrying P_{Nanog}-GFP-T2A-Luc transgene (shown in Fig. 3B,C) by FACS. Error bars represent as mean ± SD (**p* < 0.05, ***p* < 0.01 compared to GFP⁻ cells).

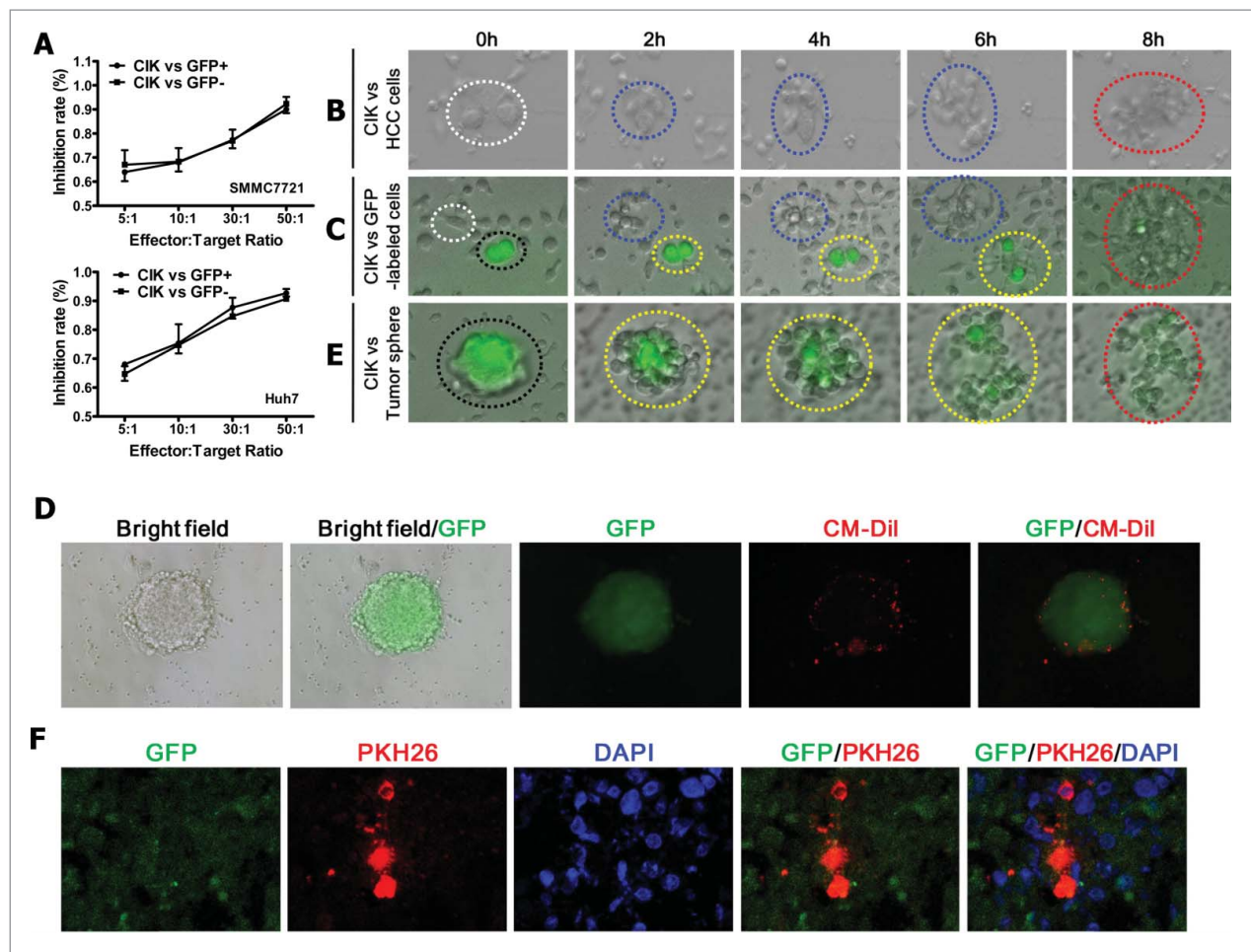


Figure 4. CIK cells have direct killing effect on stem-like cancer cells of HCC (A) The antitumor activity of CIK cells was equally intense against GFP(+) and GFP(-) HCC cells. (B) Time-lapse imaging (see Movie S1) used to observe the interactions between SMMC7721 cells and CIK cells. Representative time-lapse images are shown in (B). The white-dashed circles enclose cancer cells. Cancer cells surrounded by these blue-dashed circles were being scavenged by CIK cells, while cancer cells situated in the red-dashed circle had been scavenged by CIK cells. (C) Time-lapse imaging (see Movie S2) used to observe the interactions between SMMC7721 cells harboring P_{Nanog} -GFP-T2A-Luc transgene and CIK cells. Representative time-lapse images are shown in (C). The black- and white-dashed circles enclose GFP+ and GFP- cancer cells, respectively. GFP+ and GFP- cancer cells surrounded by yellow- and blue-dashed circles, respectively, were scavenged by CIK cells, while GFP+ and GFP- cancer cells surrounded by red-dashed circle had been scavenged by CIK cells. (D) Representative pictures of GFP(+) tumor sphere surrounded by CM-Dil-labeled CIK cells. GFP(+) tumor spheres were generated from GFP+ cells sorted from SMMC7721 cells harboring P_{Nanog} -GFP-T2A-Luc transgene. Red fluorescent dye CM-Dil was used to label CIK cells. (E) Time-lapse imaging (see Movies S3) used to observe the interactions between GFP+ tumor spheres (derived from GFP+ cells sorted from SMMC7721 cells harboring P_{Nanog} -GFP-T2A-Luc transgene) and CIK cells. Representative time-lapse images are shown in (E). The black-dashed circle encloses GFP+ tumor sphere. GFP+ tumor sphere surrounded by yellow-dashed circles was scavenged by CIK cells, while GFP+ tumor sphere situated in the red-dashed circle had been scavenged by CIK cells. (F) Infiltration of PKH26-labeled CIK cells surrounding GFP+ stem-like cancer cells was shown by red fluorescence in frozen tissue section. GFP+ cells sorted from SMMC7721 cells harboring P_{Nanog} -GFP-T2A-Luc transgene were subcutaneously injected into the dorsal thigh of NOD/SCID mice. After implanted tumor formed, CIK cells labeled with red fluorescent dye PKH26 were injected intravenously once every day. Three days later, mice were sacrificed, and tumors were dissected, followed by frozen section. Error bars represent as mean \pm SD.

GFP+ or GFP- cells was often attacked simultaneously by many CIK cells and finally killed by CIK cells (Movie S2).

As tumor-derived spheres are highly enriched in CSCs, the time-lapse fluorescence recording system was further employed to visualize the killing process of CIK cells against tumor sphere of HCC.^{31,32} As shown in Fig. 4D, GFP+ tumor sphere was surrounded by many CM-Dil-labeled CIK cells with red fluorescence when CM-Dil-labeled CIK cells were added into culture dish with GFP+ tumor spheres. Time-lapse fluorescence video microscopy revealed that one GFP+ tumor sphere exhibiting green fluorescence from GFP was attacked simultaneously by many CIK cells (Fig. 4E and Movie S3). During the process of the continuous attack and killing of CIK cells, the GFP+ tumor sphere gradually became

smaller and its shape became irregular, until cancer cells within GFP+ tumor sphere were killed completely, while green fluorescence emitted from cancer cells became more and more weak, until the green fluorescence from GFP disappeared completely at the indicated time range (Fig. 4E and Movie S3). Moreover, complete or near-complete loss of fluorescence in the most right picture of Fig. 4E demonstrated that cancer cells within GFP+ tumor sphere in the most left picture of Fig. 4E had been scavenged by CIK cells. Further *in vivo* analysis established that red fluorescence-labeled CIK cells could infiltrate tumors formed from GFP+ cells sorted from SMMC7721 cells harboring P_{Nanog} -GFP-T2A-Luc transgene (Fig. 4F). Together, our findings strongly suggest that CIK cells are active against putative CSCs of HCC.

CIK cells killed stem-like cancer cells of HCC via NKG2D-ligands recognition

The MHC-unrestricted tumor-killing activity of CIK cells is mainly mediated by the interaction of their membrane receptor NKG2D with stress-inducible molecules, MIC A/B and ULBPs, on target cells.^{6,39,40} Our aforementioned results revealed that the antitumor activity of CIK cells were equally intense against putative CSCs and non-CSCs of HCC. Therefore, the blocking assay of anti-NKG2D antibody was used to define whether CIK cells might kill putative CSCs of HCC by NKG2D-ligands recognition.

First, we observed that addition of anti-NKG2D neutralizing antibody partially but significantly rescued the reduced colony formation ability (Fig. 5A) and tumor sphere formation ability (Fig. 5B) of CIK-treated SMMC7721 and Huh7 cells, suggesting that NKG2D blockade partially blocked tumor-killing activity of CIK cells.

Subsequently, we employed GFP+ putative CSCs sorted from SMMC7721 and Huh7 cells harboring P_{Nanog}-GFP-T2A-Luc transgene to evaluate whether addition of anti-NKG2D antibody could inhibit the direct killing effect of CIK cells against putative CSCs of HCC by colony formation assay and tumor sphere formation assay. Our results showed that addition of anti-NKG2D antibody significantly but partially

restored the remarkably reduced colony formation ability (Fig. 5C) and tumor sphere formation ability (Fig. 5D) of CIK-treated GFP+ putative CSCs of SMMC7721 and Huh7 cells, suggesting that NKG2D blockade partially inhibited the direct tumor-killing effect of CIK cells against putative CSCs of HCC.

Additionally, CCK8 assay exhibited that addition of anti-NKG2D antibody led to the remarkable decrease in tumor-killing efficiency of CIK cells against putative CSCs of HCC by 12.6% and 18.2% at 30:1 and 50:1 E:T ratio (for SMMC7721-GFP+)(Fig. 5E), and by 25.2%, 27.8% and 17.7% at 10:1, 30:1 and 50:1 E:T ratio (for Huh7-GFP+)(Fig. 5E), respectively, compared with controls.

All these results certainly indicate that the direct tumor-killing activity of CIK cells against putative CSCs of HCC, at least in part, by NKG2D-ligands recognition.

CIK-treated GFP+ HCC cells exhibited significantly increased apoptotic cells

Our results showed that CIK cells efficiently killed cancer cells at least by both NKG2D-ligands recognition (Fig. 5) and effector cytokines secreted by CIK cells (Supplemental Results and Fig. 6E). Next, the apoptosis of putative CSCs and non-CSCs induced by CIK cells was examined by TUNEL staining.

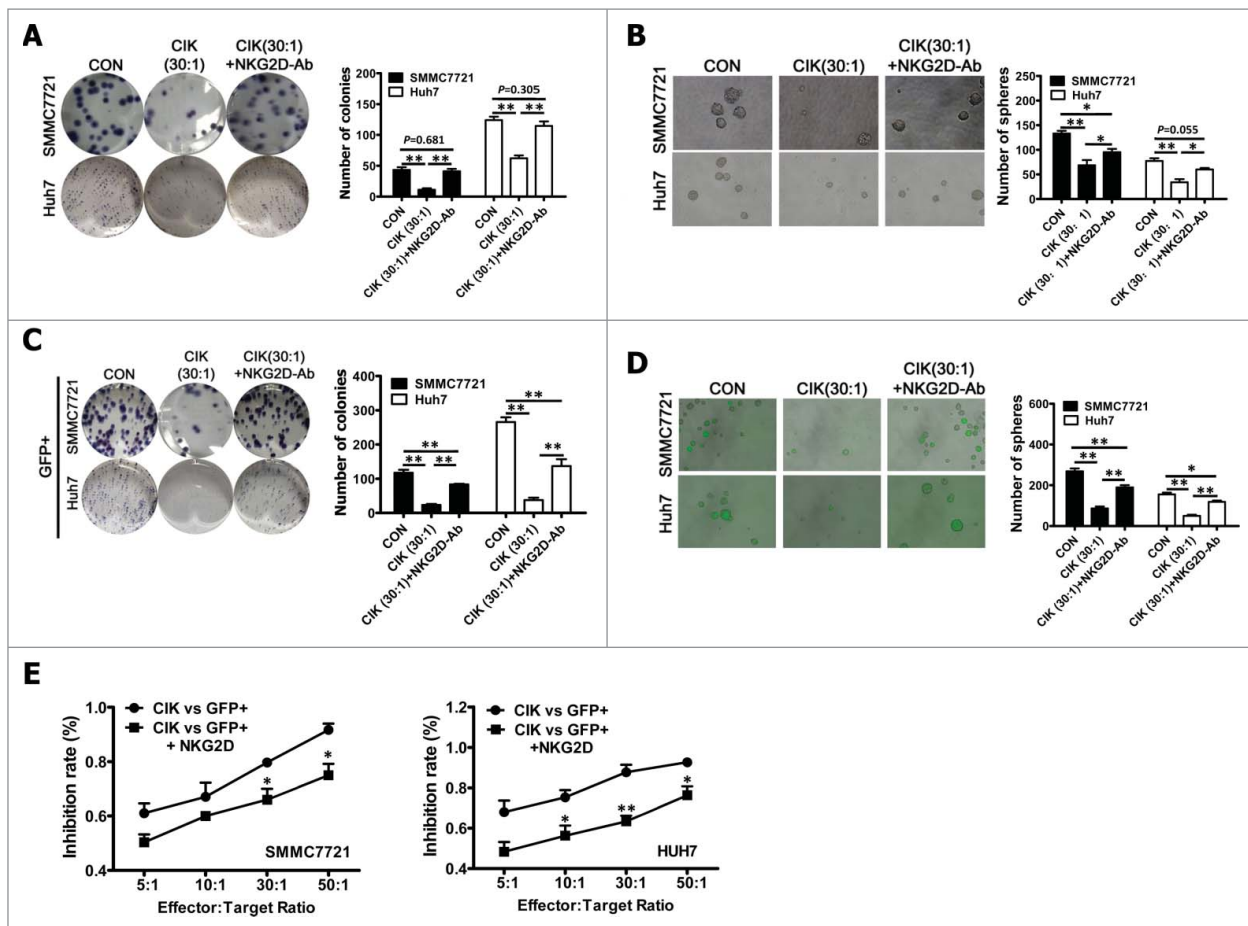


Figure 5. Blocking of NKG2D with antibody significantly reduced tumor killing activity of CIK cells. (A–B) Colony formation assay (A) and tumor sphere formation assay (B) of SMMC7721 and Huh7 cells treated with CIK cells alone and CIK cells which were pre-incubated with anti-NKG2D antibody for 30 min. (C–E) Colony formation assay (C), tumor sphere formation assay (D) and CCK8 assay (E) of GFP+ cells (sorted from SMMC7721 and Huh7 cells harboring P_{Nanog}-GFP-T2A-Luc transgene) treated with CIK cells alone and CIK cells which were pre-incubated with anti-NKG2D antibody for 30 min. Error bars represent as mean ± SD (**p* < 0.05, ***p* < 0.01).

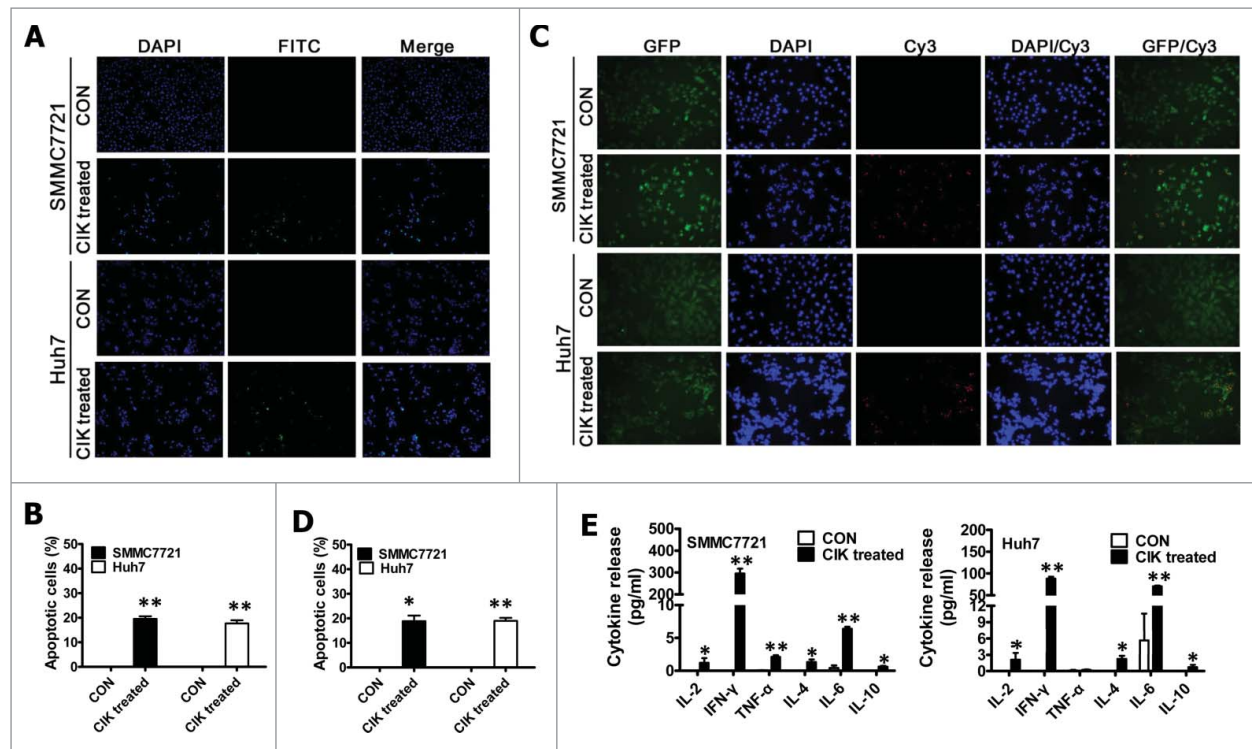


Figure 6. CIK cells efficiently killed HCC cells (including putative CSCs) through the induction of apoptosis and secretion of immune cytokines. (A–B) CIK-treated SMMC7721 and Huh7 cells exhibited significantly increased apoptotic cells detected by TUNEL staining. (C–D) CIK-treated GFP+ SMMC7721 and Huh7 cells showed significantly enhanced apoptotic cells assayed by TUNEL staining. After SMMC7721 and Huh7 cells (A–B) or GFP+ fractions sorted from SMMC7721 and Huh7 cells carrying P_{Nanog} -GFP-T2A-Luc transgene by FACS (C–D) were co-cultured with CIK cells for 24 h, cancer cells were washed three or four times with PBS to fully remove suspended CIK cells, followed by TUNEL staining to detect cells undergoing apoptosis. The FITC-conjugated green signal (A) and Cy3-conjugated red signal (C) showed the presence of TUNEL-positive cells. DAPI (blue) is used as nuclear counterstain. (E) The levels of IL-2, IL-4, IL-6, IL-10, TNF- α and IFN γ in 24 h co-culture supernatant were determined by ELISA. Error bars represent as mean \pm SD (* p < 0.05, ** p < 0.01 compared to controls without CIK cell treatment).

TUNEL staining revealed about $19.5 \pm 1.9\%$ and $17.7 \pm 2.2\%$ of apoptotic cells in SMMC7721 and Huh7 cells exposed to CIK cells (Fig. 6A,B). Moreover, GFP+ putative CSCs of HCC were also treated for 24 h with CIK cells, and subsequently TUNEL analysis showed that CIK cell treatment led to the significant increased apoptosis in GFP+ putative CSCs (Fig. 6C, D). In contrast, few apoptotic cells were observed in the corresponding control cells untreated with CIK cells (Fig. 6C,D). Summarily, our studies suggest that CIK cells efficiently kill putative CSCs and non-CSCs of HCC by inducing apoptosis.

In vivo bioluminescence imaging of antitumor activity of CIK cells against putative CSCs of HCC

These above-mentioned *in vitro* findings strongly demonstrated that both putative CSCs and non-CSCs of HCC could be attacked and efficiently killed by CIK cells, as shown by various efficient *in vitro* approaches. We next evaluated the tumor-killing activity of CIK cells *in vivo* against putative CSCs of HCC in NOD/SCID mice by *in vivo* optical imaging and other methods.

For *in vivo* bioluminescence imaging of putative CSCs, NOD/SCID mice were subcutaneously implanted with the newly established SMMC7721 cell line harboring P_{Nanog} -GFP-T2A-Luc transgene. One week after SMMC7721 cell implantation, CIK cells were injected intravenously into tumor-bearing NOD/SCID mice once every day at doses of 1×10^7 and 3×10^7 cells per mouse, followed by the indicated detections and

analyses described below. Following CIK cell treatment, a significant reduction of tumor growth was observed in CIK-treated mice (CIK cell dose: 3×10^7), but not in CIK-treated mice (CIK cell dose: 1×10^7), compared with untreated controls (Fig. 7D).

On day 13, all tumors were collected from NOD/SCID mice and weighed, which demonstrated the strong antitumor effects of CIK cells against SMMC7721 cells (Fig. 7E, F), followed by histological analysis and immunohistochemical analysis. CIK cells that were injected intravenously at doses of 3×10^7 cells per mouse inhibited tumor weight by 44.3% (Fig. 7F). Additionally, the control and CIK cell-injected NOD/SCID mice exhibited body weight gains of 115–123%, and no difference in body weight of NOD/SCID mice was found between the CIK-treated and the control mice, suggesting that CIK cell therapy did not produce animal toxicity. The results of immunohistochemical analysis revealed that the number of hyperproliferative BrdU- and Ki67-positive tumor cells in two CIK-treated groups were significantly decreased compared with control (Fig. 7G), while the percentages of BrdU- and Ki67-positive tumor cells between two CIK-treated groups became statistically significant (Fig. 7G).

More importantly, tumor-bearing NOD/SCID mice were imaged at the indicated time points by *in vivo* bioluminescence imaging to monitor the changes in the number of putative CSCs within tumor xenografts. Series of *in vivo* bioluminescence and fluorescence images taken of three representative

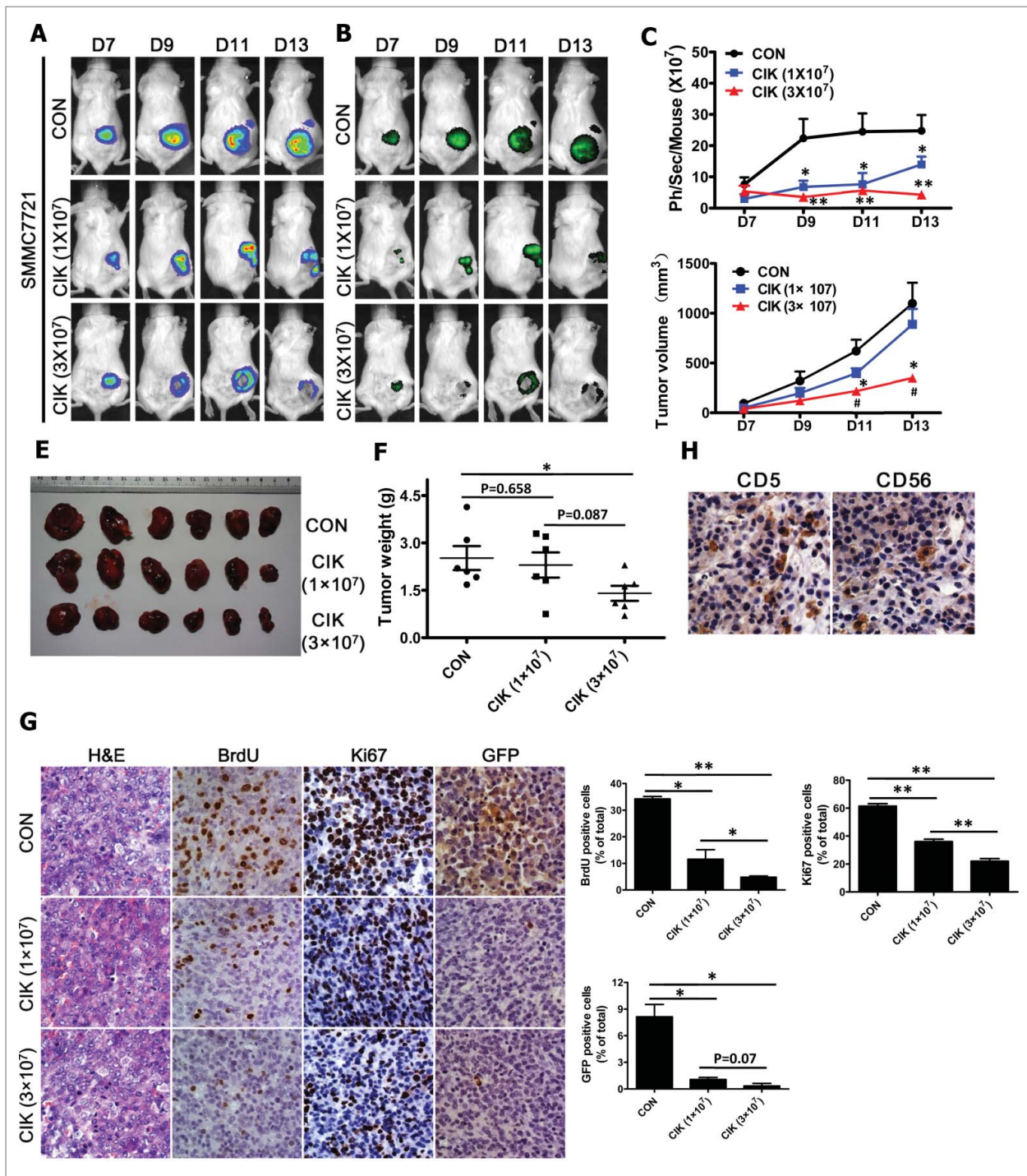


Figure 7. *In vivo* activity of CIK cells against SMMC7721 cells harboring GFP-T2A-Luc in NOD/SCID mice. As mentioned in Materials and methods section, NOD/SCID mice were subcutaneously implanted with 1×10^6 SMMC7721 cells harboring P_{Nanog} -GFP-T2A-Luc transgene. Seven days after tumor cell implantation, 1×10^7 and 3×10^7 CIK cells were infused by tail vein injection into recipient mice once every day. (A–B) Series of *in vivo* bioluminescence (A) and fluorescence (B) images (taken at the indicated times) of three representative NOD/SCID mice from CIK- (1×10^7), CIK- (3×10^7) and vehicle-treated groups before and after CIK cell treatment. (C) Quantification analysis of bioluminescence signal of tumor-bearing mice treated with CIK cells (1×10^7 and 3×10^7) or with vehicle control. (D) Growth curve of tumor volumes. (E) Representative picture of tumors formed. (F) Tumors were weighed. (G) BrdU, Ki67 and GFP-stained sections of transplanted tumors formed by SMMC7721 cells at 13 d after subcutaneous transplantation. The percentages of BrdU-, Ki67- or GFP-positive cancer cells were calculated by the total number of BrdU-, Ki67- or GFP-positive cells over total number of cancer cells. (H) Infiltration of CIK cells at tumor sites was shown by immunohistochemistry (Ab anti-CD5 and Ab anti-CD56) at the end of experiment. Error bars represent as mean \pm SD (* $p < 0.05$; ** $p < 0.01$ compared to controls without CIK cell treatment, # $p < 0.05$ compared to CIK (1×10^7) group in Fig. 7D).

mice from each group are presented in Fig. 7A,B, while quantification of the bioluminescence signal generated from each tumor-bearing mouse is shown in Fig. 7C. As shown in Fig. 7A, C, following CIK cell treatment, the significant reduction of bioluminescence signal was found in CIK-treated mice

compared with untreated controls, indicating that a general downward trend in the number of putative CSCs within tumor xenografts after CIK cell treatment can be readily, noninvasively and optically monitored by *in vivo* bioluminescence imaging.

In addition, as the expression of both GFP and Luc transgenes in tumor xenografts is driven by the same Nanog promoter, we intended to further quantify number of putative CSCs by determining the percentage of GFP-positive cells in the paraffin-embedded section of tumor xenografts via GFP antibody-based staining method. As shown in Fig. 7G, GFP antibody-based staining of tumor xenografts exhibited that the significant decreases in the percentage of GFP-positive cells were found in CIK-treated mice compared with untreated controls, suggesting a general downward trend in the number of putative CSCs within tumor xenografts after CIK cell treatment. Thus, the significant decrease of bioluminescence signal (Fig. 7A,C) in CIK-treated mice correlated well with the remarkable reduction in the percentage of GFP-positive cells (Fig. 7G). Together, these findings from both *in vivo* bioluminescence imaging and GFP antibody-based staining clearly demonstrate that CIK cells treatment leads to the remarkable reduction in the number of putative CSCs within tumor xenografts in NOD/SCID mice, indicating that CIK cells can efficiently kill putative CSCs *in vivo*, which is likely responsible for the significant tumor growth suppression in the mouse xenograft model after CIK cell treatment. Additionally, CD5 and CD56 immunohistochemistry assays confirmed the presence of CIK cells infiltrating the tumors formed from SMMC7721 cells (Fig. 7H).

Discussion

Our study showed the *in vitro* and *in vivo* intense tumor-killing activity of CIK cells toward putative HCC CSCs, as fully revealed by various efficient *in vitro* and *in vivo* methods mentioned above. Furthermore, recent studies reported the preclinical tumor killing activity of patient-derived CIK cells against putative CSCs of autologous metastatic melanoma,²⁴ and autologous metastatic bone sarcoma and soft-tissue sarcomas,²⁵ as only shown by *in vitro* little evidences (i.e., visualizing putative CSCs within *in vitro* cultured cancer cells by Oct4 promoter-GFP fluorescence reporter gene strategy, and antitumor activity assay of CIK cells against GFP+ putative CSCs), which is still required to be verified by the aforementioned approaches (i.e., tumor sphere formation, time-lapse imaging, and *in vivo* optically imaging and quantifying putative CSCs in tumor xenograft-bearing mice, etc.). Therefore, these preliminary findings from our study and other investigators demonstrate the intense antitumor killing activity of CIK cells against putative CSCs of HCC, melanoma, and bone sarcoma and soft-tissue sarcomas, but intensive research work still needs to be done to confirm the antitumor killing activity of CIK cells toward putative CSCs of various other tumors.^{24,25}

The strong cytotoxicity of CIK cells against HCC cells, including putative CSCs, encouraged us to examine in detail the mechanisms underlying the tumoricidal effect of CIK cells toward putative CSCs of HCC. The non-MHC-restricted tumor-killing activity of CIK cells is mainly based on the interaction between NKG2D molecules and MIC A/B or ULBPs molecules.^{6,39,40} Blocking of NKG2D receptor resulted in significant reduction of tumor-killing activity of CIK cells against cancer cells of bone sarcoma and soft-tissue sarcomas.²⁵ The tumor killing activity of CIK cells remained equally effective

against both putative CSCs and non-CSCs of HCC (this study), melanoma,²⁴ and bone sarcoma and soft-tissue sarcomas.²⁵ In this study, we firstly demonstrated the direct tumor-killing activity of CIK cells against putative CSCs of HCC, at least in part, by NKG2D-ligands recognition.

MIC A/B and ULBPs are the main, but not exclusive, ligands recognized by CIK cells; other molecules may be implicated.⁷ This could explain the significant reduction but not abrogation of the cytotoxicity of CIK cells observed blocking NKG2D receptor in our study (Fig. 5). A more complete definition of all tumor ligands recognized by CIK cells, their setting of expression and different role in mediating the cytotoxicity of CIK cells may help the identification of subsets of cancer patients that could better benefit from CIK cell-based immunotherapy, suggesting the potential clinical relevance deserving dedicated investigations.

Cumulating evidence has revealed that CSCs are thought to play a pivotal role in tumor maintenance, metastasis, therapy resistance and relapse.^{41,42} Thus, the development of methods for *in vitro* optical imaging and non-invasive *in vivo* detection of putative CSCs is of great importance.^{43,44} The commonly used optical molecular imaging techniques include fluorescence and bioluminescence imaging which have their own advantages.⁴³⁻⁴⁵

Currently, the promoter-fluorescence reporter gene strategy has successfully been employed to *in vitro* optical image putative CSCs in a live population of HCC,³⁸ melanoma,²⁴ and bone and soft-tissue sarcomas cells.²⁵ In the aforementioned promoter-reporter gene assay, cancer cells harboring GFP gene under control of a stem cell-specific Oct4²⁴⁻²⁵ or Nanog promoter³⁸ were employed to realize optical tracking putative CSCs within a population of *in vitro* cultured cancer cells by *in vitro* fluorescence imaging.

Compared with *in vivo* fluorescence imaging, *in vivo* bioluminescence imaging possesses high spatial resolution and sensitivity and high tissue-penetration depths, and has successfully been used to optically and non-invasively monitor tumor growth, regression and metastasis.⁴³⁻⁴⁵ Therefore, *in vivo* bioluminescence imaging should provide the greatest advantage at *in vivo* optically imaging, tracking and quantifying small numbers of cells (i.e., putative CSCs) in human tumor xenograft-bearing mice. It is very clear that multimodality imaging approaches may minimize the potential drawbacks of using each imaging modality alone and a tailored combination of two or more imaging techniques, such as fluorescence and bioluminescence imaging, may be the best approach for a given experiment.⁴³⁻⁴⁵ Therefore, we firstly developed a new methodology to *in vitro* and *in vivo* visualize putative CSCs based on a lentiviral "CSC detector" vector encoding the copGFP and Luc proteins regulated by the promoter of stem gene Nanog, which has never been reported previously. Our data from various experimental methods exhibited that GFP+ cancer cells harboring P_{Nanog}-GFP-T2A-Luc transgene exhibit the characteristics of CSCs. In this study, GFP+ cancer cells (i.e., putative CSCs) were sorted from HCC cells harboring P_{Nanog}-GFP-T2A-Luc transgene to be further used in various experiments mentioned above. Furthermore, by time-lapse video imaging, the newly established HCC cell lines harboring P_{Nanog}-GFP-T2A-Luc transgene allows us to *in vitro* visualize the whole killing

process of CIK cells against cancer cells, including GFP+ putative CSCs (Fig. 4), which has never been reported previously. On the other hand, the noninvasive *in vivo* bioluminescence imaging allowed us to readily and optically monitor, for the first time, the remarkable reduction in the number of putative CSCs within tumor xenografts in NOD/SCID mice after CIK cell treatment, which was correlated well with the remarkable reduction in the percentage of GFP-positive cells detected by GFP antibody-based staining method. Therefore, the HCC cell line harboring double reporter genes GFP and Luc under control of a stem cell-specific Nanog promoter allows us to *in vitro* visualize putative CSCs and to *in vivo* optically image and quantify putative CSCs within tumor xenograft-bearing mice, which has never been reported in other cancers.

As mentioned above, time-lapse imaging provides us a better understanding of the killing process of CIK cells against HCC cells, including putative CSCs or tumor spheres. In this study, time-lapse video microscopy fully revealed that when CIK cells were *in vitro* co-cultured with them, each of cancer cells, GFP-labeled putative CSCs, or tumor spheres in which CSCs are enriched was usually attacked simultaneously by many CIK cells and finally killed by CIK cells, suggesting that it is very necessary to achieve sufficient effector to target ratios if cancer cells, including putative CSCs and tumor spheres, are expected to be efficiently killed by CIK cells *in vitro* and *in vivo*. Summarily, our present study firstly illustrated the killing whole process of CIK cells against putative CSCs or tumor spheres by using time-lapse video recording.

As mentioned above, the failure of current anticancer therapies can be attributed to the relative ineffectiveness of drug and radiation treatments on CSCs, but the development of new therapeutic strategies targeting CSCs is currently hindered by the lack of reliable markers for the identification of these CSCs.¹⁴⁻²² Additionally, there is an urgent need for more potent and safer therapies against CSCs for curing the cancer with no or minimal damage to the surrounding normal tissue, but a major hurdle to this goal lies in the identification of the key mechanisms that distinguish CSCs from the normal endogenous tissue stem cells.¹⁴⁻²² One of the major advantages of most immunotherapeutic strategies (e.g., CIK cell-based anti-cancer immunotherapy) is relatively low or acceptable toxicity against the normal tissues and cells, in contrast to traditional chemotherapy and radiotherapy, whereas the data from this study and other investigators demonstrated that CIK cell-based immunotherapy for cancer showed high tumor killing activity against cancer cells, including CSCs.^{7,23-25,46} Therefore, CIK cell-based therapeutic strategies against CSCs present a promising and safely immunotherapeutic approaches for cancer treatment.

CIK cell therapy for cancer patients shows the attractive advantages over other adoptive immunotherapies,^{7,47,48} but several strategies have been adopted to enhance CIK cell function and improve the antitumor efficacy of CIK cells.⁷ These strategies include the use of chimeric antigen receptors (CARs)⁴⁹⁻⁵⁴ and bispecific antibodies (BsAb)⁵⁵⁻⁵⁹ to re-direct CIK cells toward specific cancer targets. CAR-engineered CIK cells resulted in more efficient tumor cell lysis.^{7,49-54}

The advantages of CIK cell therapy over other types of autologous T cell therapies including CAR T cells are the

effective tumor-homing abilities and recognition of stress ligands, not tumor-specific antigens, for tumor cell killing.⁷ These extend the therapeutic value to numerous types of cancer including solid tumors. Applying CARs to CIK cells improves specific tumor killing; however, will still not overcome the effector to target ratio problem,⁷ indicating that there is an urgent need for the approaches to achieving sufficient effector to target ratios.

Overall, our *in vitro* and *in vivo* results illustrate the intense tumor killing activity of CIK cells against putative CSCs of HCC, suggesting that immune targeting of CSCs presents a promising approach for cancer treatment. Our findings encourage us to further examine the antitumor activity of HCC patient-derived CIK cells against autologous HCC and the elusive subset of putative CSCs. On the other hand, we will perform further preclinical and clinical investigations on the prospective potential of targeting putative CSCs of HCC with CIK cells in synergism with other therapeutic strategies (e.g., RFA and/or TACE) because the immunotherapy often needs to be accompanied by traditional treatment strategies such as RFA and/or TACE. CIK cell-based immunotherapy for cancer is becoming a fascinating tool in the fight against cancer, and its further development in the near future is guaranteed.

Materials and methods

Cell lines and cell culture

Human HCC cell lines SMMC7721 and Huh7 were purchased from the Cell Bank of the Chinese Academy of Sciences (Shanghai, China). These cells were cultured in Dulbecco's modified Eagle's medium (DMEM) supplemented with 10% fetal bovine serum (FBS) (Biological Industries) in a humidified incubator with 5% CO₂ at 37°C.

CIK culture, expansion and phenotype analysis

Human peripheral blood samples were obtained from healthy donors. All individuals provided their informed consent. PBMCs were separated from heparinized peripheral blood samples by Ficoll-Hypaque density gradient centrifugation and subsequently washed twice with PBS. Next, PBMCs were cultured overnight in cell culture flasks at a cell density of 2×10^6 cells/mL in RPMI 1640 (Corning) supplemented with 10% FBS in 100 U/mL IFN γ (Shanghai Kaimao, China) and 10 μ g/mL Polyhydroxyalkanoates (PHA) (Huizhou Hongyu, China). After 24 h in cultured at 37°C and 5% CO₂, 50 ng/mL anti-CD3 antibody (Miltenyi, Germany) and 1000 U/mL recombinant human interleukin-2 (IL-2) (Beijing Sihuan, China) were added. Fresh medium with IL-2 and anti-CD3 antibody was added as needed. Cells were expanded over 3 weeks of time period. Cells were obtained from CIK cell cultures for phenotype analysis with the appropriated monoclonal antibodies (mAb), including CD3-FITC, CD4-FITC, CD8-PE, CD56-APC, and CD314-APC (anti-NKG2D) (Miltenyi, Germany) by standard flow cytometric assays (BD Biosciences).

CCK8 assay and colony formation assay

CCK8 assay was used to evaluate the cytotoxic activity of CIK cells against cancer cells. Briefly, HCC cells were co-cultured in 96-well plates with CIK cells at specified effector: target ratios (5:1, 10:1, 30:1 and 50:1) in a final volume of 200 μ L for 4 h. Tumor cells alone and CIK cells alone were used as the target cells alone group (blank control group) and the effector cells alone group, respectively. The kill rate was calculated according to the formula: inhibition rate (100%) = $[1 - (A \text{ value in experimental well} - A \text{ value in effector cell wells}) / A \text{ value in target cell wells}] \times 100\%$.

After HCC cells were co-cultured with CIK cells at specified effector: target ratios (5:1, 10:1, 30:1 and 50:1) for 24 h, HCC cells were washed three or four times with PBS to fully remove the suspended CIK cells, and then used for colony formation assay. Colony formation assay was previously fully described.²⁶

Transwell migration assay and Boyden invasion assay

After HCC cells were co-cultured with CIK cells at specified effector: target ratio (10:1) for 24 h, HCC cells were washed three or four times with PBS to fully remove the suspended CIK cells, and subsequently collected and counted for transwell migration assay and Boyden invasion assay, as described previously.²⁷

Sphere formation assay

To assess sphere formation efficiency, HCC cells treated with CIK cells at different effector: target ratios for 24 h were collected and counted. Next, the 9000 cells were subsequently plated in ultra-low attachment six-well plates and cultured in Dulbecco's modified Eagle's medium/F12 (Hyclone) supplemented with B27 supplement (1:50 dilution; BD), 20 ng/mL epidermal growth factor (PeproTech) and 10 ng/mL basic fibroblast growth factor (PeproTech). After one week of culture, tumor spheres were counted under an inverted microscope.

Plasmids and lentivirus vector construction

The plasmid of pL-SIN-P_{Nanog}-EGFP, carrying human Nanog promoter, was obtained from Addgene (plasmid 21321). The lentivirus vector of pOct4CR4-pGreenFire1TM EF1-Puro Response Reporter (SR20070-PA-P) was purchased from System Biosciences (SBI). The lentiviral packaging plasmids psPAX2 and pMD2.G were kindly provided by Prof. Didier Trono (University of Geneva, Geneva, Switzerland).

Human Nanog promoter fragment were amplified from pL-SIN-Nanog-EGFP, and then directly inserted into *EcoR* I and *Bam*H I sites of pOct4CR4-pGreenFire1TM EF1-Puro to generate pLV-P_{Nanog}-GFP-T2A-Luc. This complete sequence of human Nanog promoter fragment was confirmed through DNA sequencing. Thus, the resultant plasmid of pLV-P_{Nanog}-GFP-T2A-Luc harbors both the reporter genes [i.e., GFP and luciferase (Luc)] under control of Nanog promoter and puromycin resistance gene under control of EF-1 α promoter.

Lentivirus production and transduction

To generate stable cell lines, recombinant lentiviruses (named as LV-P_{Nanog}-GFP-T2A-Luc) were generated as previously described,²⁸ and subsequently used to infect SMMC7721 and Huh7 cells. Next, stable infected cells were selected with puromycin in 4 μ g/mL concentration to establish puromycin-resistant stable reporter cell lines (i.e., SMMC7721 cells and Huh7) carrying P_{Nanog}-GFP-T2A-Luc transgene, followed by GFP assay via inverted fluorescence microscope (Nikon, Japan) and flow cytometry. Moreover, GFP+ and GFP- fractions were sorted for subsequent experiments by fluorescence-activated cell sorting (FACS) (BD FACSAria).

RNA isolation and quantitative real-time PCR (qRT-PCR)

RNA isolation and qRT-PCR were previously well described.²⁷ The primers used in qRT-PCR assay were listed in Table S1.

PKH26 and CM-Dil labeling of CIK cells

In some experiments of this study, to distinguish the CIK cells from GFP-labeled tumor cells, red fluorescent dyes, including PKH26 (Sigma-Aldrich) and CM-Dil (Sigma-Aldrich), were used to label CIK cells, according to the instructions provided by the manufacturer.

Time-lapse recording

In order to observe the interactions between cancer cells or tumor spheres and CIK cells, live cell imaging were taken using an incubator microscope system (LumaScope model 600, Etaluma, USA). Image acquisition was started immediately after CIK cells were added into culture dish. Images were captured every 2 min for 8 h (cells) or 4 min for 24 h (tumor spheres). These images were processed using the LumaView 600 software (Etaluma, USA).

NKG2D blockade assays

To examine the mechanisms underlying the tumoricidal effect of CIK cells, CIK cells were firstly exposed to mAbs against human NKG2D (Clone #552866, BD PharMingen) (20 μ g/mL) for 30 min, and then co-cultured with HCC cells for 24 h, followed by CCK8 assay, colony formation assay or tumor spheroid assay.

TUNEL staining assay

After HCC cells were treated with CIK cells for 24 h, cells were washed three or four times with PBS to fully remove suspended CIK cells, dried at room temperature, fixed with 4% formalin for 15 min, and then underwent TUNEL staining by using the TUNEL Apoptosis Detection Kit (KeyGEN BioTECH) following the manufacturer's protocol.

Cytokine production assay

HCC cells were co-cultured with CIK cells for 24 h in six-well culture plate. Twenty-four hours after co-culture, cell culture supernatants were harvested and analyzed for supernatant concentrations of IL-2, IL-4, IL-6, IL-10, TNF- α and IFN γ by ELISA kit (MultiSciences, China) according to the manufacturer's instructions.

Xenograft experiments in NOD/SCID mice

The animal experiments were carried out in strict accordance with the recommendations in the Guide for the Care and Use of Laboratory Animals of the Southern Medical University. The animal protocol was approved by the Committee on Ethics of Animal Experiments of the Southern Medical University. Female NOD/SCID mice aged 4 to 5 weeks were purchased from the Model Animal Research Center of Nanjing University, and housed in microisolator cages under aseptic conditions. SMMC7721 cells (1×10^6 cells) harboring P_{Nanog}-GFP-T2A-Luc transgene were resuspended in a mix of PBS and BD Matrigel (BD Biosciences) (1:1), and then subcutaneously injected into the right or left dorsal thigh of mice. One week after SMMC7721 cell implantation, the mice were treated with 1×10^7 CIK cells, 3×10^7 CIK cells or PBS as the untreated control via tail vein injection once every day. Tumor growth was determined by caliper measurement or *in vivo* bioluminescence (BLI) and fluorescence imaging (see below). Tumor volumes were calculated as previously described.⁶⁰ On day 13 after cancer cell implantation, mice were sacrificed, and tumors were dissected, weighed and fixed overnight in 4% paraformaldehyde, dehydrated, paraffin-embedded, sectioned. To determine the animal toxicity, the body weights of the animals were measured. All surgery was performed under sodium pentobarbital anesthesia, and all efforts were made to minimize suffering of animals.

Whole-animal bioluminescence and fluorescence imaging

The procedure for *in vivo* bioluminescence and fluorescence imaging via using the Xenogen IVIS LuminaII Imaging System (Xenogen Corp., Alameda, CA, USA) to noninvasively measure Luc activity and GFP was previously fully described.^{29,30}

Histological and immunohistological examinations

For immunohistology analysis, tumor tissues were fixed with 4% paraformaldehyde (PFA) in PBS, embedded in paraffin, cut into 5 μ m thick sections, and then deparaffinized, followed by hematoxylin and eosin staining (H&E staining) according to standard procedures. After deparaffinization and rehydration, the paraffin-embedded sections were subjected to high pressure for 2 min for antigenic retrieval. The slides were incubated overnight at 4°C with the indicated primary antibodies (Table S2).

Statistical analysis

All data were shown as mean \pm SD. Statistical analysis was conducted using a SPSS 13.0 software package and Graphpad 5.0 software. Independent-Sample *t* test was used for comparisons

of two independent groups. The One-Way ANOVA was used for compare comparisons of multiple groups. The mixed model analysis of variance (ANOVA) was employed to assess CIK cytotoxic activity curves *in vivo*. Values are statistically significant at * or # $p < 0.05$; ** or ## $p < 0.01$.

Disclosure of potential conflicts of interest

No potential conflicts of interest were disclosed.

Funding

This work was supported by the National Natural Science Foundation of China (Grant No. 81172587 and 81372896, to D. Xiao; Grant No. 61427807), the Natural Science Foundation of Guangdong Province of China (Grant No. 2014A030313294 to D. Xiao; Grant No. 9151063101000015, to J.-S. Jia), the Science and Technology Planning Project of Guangdong Province of China (Grant No. 2009B060300008 and 2013B0603000013, to D. Xiao), National High Technology Research and Development Program of China (Program 863) (Grant No. 2012AA02A501) and the Introduced Major Research and Development Project Funded by Fujian Province (Grant No. 2012I2014).

References

1. Padma S, Martinie JB, Iannitti DA. Liver tumor ablation: percutaneous and open approaches. *J Surg Oncol* 2009; 100:619-34; PMID:20017157; <http://dx.doi.org/10.1002/jso.21364>
2. Sutherland LM, Williams JA, Padbury RT, Gotley DC, Stokes B, Madern GJ. Radiofrequency ablation of liver tumors: a systematic review. *Arch Surg* 2006; 141:181-90; PMID:16490897; <http://dx.doi.org/10.1001/archsurg.141.2.181>
3. Llovet JM, Bruix J. Systematic review of randomized trials for unresectable hepatocellular carcinoma: Chemoembolization improves survival. *Hepatology* 2003; 37:429-42; PMID:12540794; <http://dx.doi.org/10.1053/jhep.2003.50047>
4. Avila MA, Berasain C, Sangro B, Prieto J. New therapies for hepatocellular carcinoma. *Oncogene* 2006; 25:3866-84; PMID:16799628; <http://dx.doi.org/10.1038/sj.onc.1209550>
5. Takayama T, Sekine T, Makuuchi M, Yamasaki S, Kosuge T, Yamamoto J, Shimada K, Sakamoto M, Hirohashi S, Ohashi Y, et al. Adoptive immunotherapy to lower postsurgical recurrence rates of hepatocellular carcinoma: a randomised trial. *Lancet* 2000; 356:802-7; PMID:11022927; [http://dx.doi.org/10.1016/S0140-6736\(00\)02654-4](http://dx.doi.org/10.1016/S0140-6736(00)02654-4)
6. Sangiolo D. Cytokine induced killer cells as promising immunotherapy for solid tumors. *J Cancer* 2011; 2:363-8; PMID:21716717; <http://dx.doi.org/10.7150/jca.2.363>
7. Schmidt TL, Negrin RS, Contag CH. A killer choice for cancer immunotherapy. *Immunol Res* 2014; 58:300-6; PMID:24791943; <http://dx.doi.org/10.1007/s12026-014-8507-2>
8. Baker J, Verneris MR, Ito M, Shizuru JA, Negrin RS. Expansion of cytolytic CD8(+) natural killer T cells with limited capacity for graft-versus-host disease induction due to interferon gamma production. *Blood* 2001; 97:2923-31; PMID:11342413; <http://dx.doi.org/10.1182/blood.V97.10.2923>
9. Mesiano G, Todorovic M, Gammaitoni L, Leuci V, Giraudo Diego L, Carnevale-Schianca F, Fagioli F, Piacibello W, Aglietta M, Sangiolo D. Cytokine-induced killer (CIK) cells as feasible and effective adoptive immunotherapy for the treatment of solid tumors. *Expert Opin Biol Ther* 2012; 12:673-84; PMID:22500889; <http://dx.doi.org/10.1517/14712598.2012.675323>
10. Todorovic M, Mesiano G, Gammaitoni L, Leuci V, Giraudo Diego L, Cammarata C, Jordaney N, Carnevale-Schianca F, Gallo S, Fagioli F, et al. Ex vivo allogeneic stimulation significantly improves expansion of cytokine-induced killer cells without increasing their alloreactivity across HLA barriers. *J Immunother* 2012; 35:579-86; PMID:22892454; <http://dx.doi.org/10.1097/CJI.0b013e31826b1fd9>

11. Weng DS, Zhou J, Zhou QM, Zhao M, Wang QJ, Huang LX, Li YQ, Chen SP, Wu PH, Xia JC. Minimally invasive treatment combined with cytokine-induced killer cells therapy lower the short-term recurrence rates of hepatocellular carcinomas. *J Immunother* 2008; 31:63-71; PMID:18157013; <http://dx.doi.org/10.1097/CJI.0b013e31815a121b>
12. Zhou P, Liang P, Dong B, Yu X, Han Z, Xu Y. Phase clinical study of combination therapy with microwave ablation and cellular immunotherapy in hepatocellular carcinoma. *Cancer Biol Ther* 2011; 11:450-6; PMID:21258206; <http://dx.doi.org/10.4161/cbt.11.5.14669>
13. Huang ZM, Li W, Li S, Gao F, Zhou QM, Wu FM, He N, Pan CC, Xia JC, Wu PH, et al. Cytokine-induced killer cells in combination with transcatheter arterial chemoembolization and radiofrequency ablation for hepatocellular carcinoma patients. *J Immunother* 2013; 36:287-93; PMID:23719239; <http://dx.doi.org/10.1097/CJI.0b013e3182948452>
14. Antoniou A, Hebrant A, Dom G, Dumont JE, Maenhaut C. Cancer stem cells, a fuzzy evolving concept: a cell population or a cell property? *Cell Cycle* 2013; 12:3743-8; PMID:24270846; <http://dx.doi.org/10.4161/cc.27305>
15. Duggal R, Mineev B, Geissinger U, Wang H, Chen NG, Koka PS, Szalay AA. Biotherapeutic approaches to target cancer stem cells. *J Stem Cells* 2013; 8:135-49; PMID:24699023; <http://dx.doi.org/jsc.2014.8.3/4.135>
16. Jackson M, Hassiotou F, Nowak A. Glioblastoma stem-like cells: at the root of tumor recurrence and a therapeutic target. *Carcinogenesis* 2015; 36:177-85; PMID:25504149; <http://dx.doi.org/10.1093/carcin/bgu243>
17. Kreso A, Dick JE. Evolution of the cancer stem cell model. *Cell Stem Cell* 2014; 14:275-91; PMID:24607403; <http://dx.doi.org/10.1016/j.stem.2014.02.006>
18. Matchett KB, Lippin TR. Concise reviews: cancer stem cells: from concept to cure. *Stem Cells* 2014; 32:2563-70; PMID:25078632; <http://dx.doi.org/10.1002/stem.1798>
19. Shetzer Y, Solomon H, Koifman G, Molchadsky A, Horesh S, Rotter V. The paradigm of mutant p53-expressing cancer stem cells and drug resistance. *Carcinogenesis* 2014; 35:1196-208; PMID:24658181; <http://dx.doi.org/10.1093/carcin/bgu073>
20. Sun X, Jiao X, Pestell TG, Fan C, Qin S, Mirabelli E, Ren H, Pestell RG. MicroRNAs and cancer stem cells: the sword and the shield. *Oncogene* 2014; 33:4967-77; PMID:24240682; <http://dx.doi.org/10.1038/onc.2013.492>
21. Vidal SJ, Rodriguez-Bravo V, Galsky M, Cordon-Cardo C, Domingo-Domenech J. Targeting cancer stem cells to suppress acquired chemotherapy resistance. *Oncogene* 2014; 33:4451-63; PMID:24096485; <http://dx.doi.org/10.1038/onc.2013.411>
22. Yamashita T, Wang XW. Cancer stem cells in the development of liver cancer. *J Clin Invest* 2013; 123:1911-8; PMID:23635789; <http://dx.doi.org/10.1172/JCI66024>
23. Kwiatkowska-Borowczyk EP, Gabka-Buszek A, Jankowski J, Mackiewicz A. Immunotargeting of cancer stem cells. *Contemp Oncol* 2015; 19:A52-9; PMID:25691822; <http://dx.doi.org/10.5114/wo.2014.47129>
24. Gammaitoni L, Giraudo L, Leuci V, Todorovic M, Mesiano G, Picciotto F, Pisacane A, Zaccagna A, Volpe MG, Gallo S, et al. Effective activity of cytokine-induced killer cells against autologous metastatic melanoma including cells with stemness features. *Clin Cancer Res* 2013; 19:4347-58; PMID:23794732; <http://dx.doi.org/10.1158/1078-0432.CCR-13-0061>
25. Sangiolo D, Mesiano G, Gammaitoni L, Leuci V, Todorovic M, Giraudo L, Cammarata C, Dell'Aglio C, D'Ambrosio L, Pisacane A, et al. Cytokine-induced killer cells eradicate bone and soft-tissue sarcomas. *Cancer Res* 2014; 74:119-29; PMID:24356422; <http://dx.doi.org/10.1158/0008-5472.CAN-13-1559>
26. Wang WJ, Wu SP, Liu JB, Shi YS, Huang X, Zhang QB, Yao KT. MYC regulation of CHK1 and CHK2 promotes radioresistance in a stem cell-like population of nasopharyngeal carcinoma cells. *Cancer Res* 2013; 73:1219-31; PMID:23269272; <http://dx.doi.org/10.1158/0008-5472.CAN-12-1408>
27. Wang SC, Lin XL, Li J, Zhang TT, Wang HY, Shi JW, Yang S, Zhao WT, Xie RY, Wei F, et al. MicroRNA-122 triggers mesenchymal-epithelial transition and suppresses hepatocellular carcinoma cell motility and invasion by targeting RhoA. *PloS one* 2014; 9:e101330; PMID:24992599; <http://dx.doi.org/10.1371/journal.pone.0101330>
28. Shi JW, Liu W, Zhang TT, Wang SC, Lin XL, Li J, Jia JS, Sheng HF, Yao ZF, Zhao WT, et al. The enforced expression of c-Myc in pig fibroblasts triggers mesenchymal-epithelial transition (MET) via F-actin reorganization and RhoA/Rock pathway inactivation. *Cell Cycle* 2013; 12:1119-27; PMID:23466707; <http://dx.doi.org/10.4161/cc.24164>
29. Du T, Jia J, Lin X, Xie R, Li J, Xiao D, Xu K. Generation of Rm21LG transgenic mice: a powerful tool to generate conditional overexpression of miR-21 that is involved in oncogenesis. *Biotechnol Lett* 2014; 36:9-20; PMID:24068500; <http://dx.doi.org/10.1007/s10529-013-1327-y>
30. Lin X, Jia J, Du T, Li W, Wang X, Wei J, Lin X, Zeng H, Yao L, Chen X, et al. Overexpression of miR-155 in the Liver of Transgenic Mice Alters the Expression Profiling of Hepatic Genes Associated with Lipid Metabolism. *PloS one* 2015; 10:e0118417; PMID:25799309; <http://dx.doi.org/10.1371/journal.pone.0118417>
31. Dontu G, Abdallah WM, Foley JM, Jackson KW, Clarke MF, Kawamura MJ, Wicha MS. In vitro propagation and transcriptional profiling of human mammary stem/progenitor cells. *Genes Dev* 2003; 17:1253-70; PMID:12756227; <http://dx.doi.org/10.1101/gad.1061803>
32. Kong QL, Hu LJ, Cao JY, Huang YJ, Xu LH, Liang Y, Xiong D, Guan S, Guo BH, Mai HQ, et al. Epstein-Barr virus-encoded LMP2A induces an epithelial-mesenchymal transition and increases the number of side population stem-like cancer cells in nasopharyngeal carcinoma. *PLoS Pathog* 2010; 6:e1000940; PMID:20532215; <http://dx.doi.org/10.1371/journal.ppat.1000940>
33. Lo PK, Kanojia D, Liu X, Singh UP, Berger FG, Wang Q, Chen H. CD49f and CD61 identify Her2/neu-induced mammary tumor-initiating cells that are potentially derived from luminal progenitors and maintained by the integrin-TGFbeta signaling. *Oncogene* 2012; 31:2614-26; PMID:21996747; <http://dx.doi.org/10.1038/onc.2011.439>
34. Liu JC, Deng T, Lehal RS, Kim J, Zacksenhaus E. Identification of tumorsphere- and tumor-initiating cells in HER2/Neu-induced mammary tumors. *Cancer Res* 2007; 67:8671-81; PMID:17875707; <http://dx.doi.org/10.1158/0008-5472.CAN-07-1486>
35. Hart LS, El-Deiry WS. Invincible, but not invisible: imaging approaches toward in vivo detection of cancer stem cells. *J Clin Oncol* 2008; 26:2901-10; PMID:18539971; <http://dx.doi.org/10.1200/JCO.2008.16.9573>
36. Heryanto YD, Achmad A, Taketomi-Takahashi A, Tsushima Y. In vivo molecular imaging of cancer stem cells. *Am J Nucl Med Mol Imaging* 2015; 5:14-26; PMID:25625023
37. Sun N, Lee A, Wu JC. Long term non-invasive imaging of embryonic stem cells using reporter genes. *Nat Protoc* 2009; 4:1192-201; PMID:19617890; <http://dx.doi.org/10.1038/nprot.2009.100>
38. Shan J, Shen J, Liu L, Xia F, Xu C, Duan G, Xu Y, Ma Q, Yang Z, Zhang Q, et al. Nanog regulates self-renewal of cancer stem cells through the insulin-like growth factor pathway in human hepatocellular carcinoma. *Hepatology* 2012; 56:1004-14; PMID:22473773; <http://dx.doi.org/10.1002/hep.25745>
39. Karimi M, Cao TM, Baker JA, Verneris MR, Soares L, Negrin RS. Silencing human NKG2D, DAP10, and DAP12 reduces cytotoxicity of activated CD8+ T cells and NK cells. *J Immunol* 2005; 175:7819-28; PMID:16339517; <http://dx.doi.org/10.4049/jimmunol.175.12.7819>
40. Verneris MR, Karami M, Baker J, Jayaswal A, Negrin RS. Role of NKG2D signaling in the cytotoxicity of activated and expanded CD8+ T cells. *Blood* 2004; 103:3065-72; PMID:15070686; <http://dx.doi.org/10.1182/blood-2003-06-2125>
41. Visvader JE, Lindeman GJ. Cancer stem cells in solid tumours: accumulating evidence and unresolved questions. *Nat Rev Cancer* 2008; 8:755-68; PMID:18784658; <http://dx.doi.org/10.1038/nrc2499>
42. Visvader JE, Lindeman GJ. Cancer stem cells: current status and evolving complexities. *Cell Stem Cell* 2012; 10:717-28; PMID:22704512; <http://dx.doi.org/10.1016/j.stem.2012.05.007>
43. Hart LS, El-Deiry WS. Invincible, but not invisible: imaging approaches toward in vivo detection of cancer stem cells. *J Clin Oncol* 2008; 26:2901-10; PMID:18539971; <http://dx.doi.org/10.1200/JCO.2008.16.9573>
44. Heryanto YD, Achmad A, Taketomi-Takahashi A, Tsushima Y. In vivo molecular imaging of cancer stem cells. *Am J Nucl Med Mol Imaging* 2015; 5:14-26; PMID:25625023

45. Sun N, Lee A, Wu JC. Long term non-invasive imaging of embryonic stem cells using reporter genes. *Nat Protoc* 2009; 4:1192-201; PMID:19617890; <http://dx.doi.org/10.1038/nprot.2009.100>
46. Rong X, Wei F, Li A, Xiao D, Luo R. Effective activity of cytokine induced killer cells against hepatocellular carcinoma including tumor-initiating cells. *Med Hypotheses* 2015; 84:159-61; PMID:25636604; <http://dx.doi.org/10.1016/j.mehy.2014.08.022>
47. Kim HM, Kang JS, Lim J, Kim JY, Kim YJ, Lee SJ, Song S, Hong JT, Kim Y, Han SB. Antitumor activity of cytokine-induced killer cells in nude mouse xenograft model. *Arch Pharm Res* 2009; 32:781-7; PMID:19471894; <http://dx.doi.org/10.1007/s12272-009-1518-1>
48. Kim HM, Lim J, Yoon YD, Ahn JM, Kang JS, Lee K, Park SK, Jeong YJ, Kim JM, Han G, et al. Anti-tumor activity of ex vivo expanded cytokine-induced killer cells against human hepatocellular carcinoma. *Int Immunopharmacol* 2007; 7:1793-801; PMID:17996690; <http://dx.doi.org/10.1016/j.intimp.2007.08.007>
49. Hombach AA, Rapp G, Abken H. Arming cytokine-induced killer cells with chimeric antigen receptors: CD28 outperforms combined CD28-OX40 "super-stimulation." *Mol Ther* 2013; 21:2268-77; PMID:23985696; <http://dx.doi.org/10.1038/mt.2013.192>
50. Laurin D, Marin V, Biagi E, Pizzitola I, Agostoni V, Gallot G, Vié H, Jacob MC, Chaperot L, Asford C, et al. Upregulation of adhesion molecules on leukemia targets improves the efficacy of cytotoxic T cells transduced with chimeric anti-CD19 receptor. *J Immunother* 2013; 36:181-9; PMID:23502765; <http://dx.doi.org/10.1097/CJI.0b013e318-288f8c1>
51. Marin V, Pizzitola I, Agostoni V, Attianese GM, Finney H, Lawson A, Pule M, Rousseau R, Biondi A, Biagi E. Cytokine-induced killer cells for cell therapy of acute myeloid leukemia: improvement of their immune activity by expression of CD33-specific chimeric receptors. *Haematologica* 2010; 95:2144-52; PMID:20713459; <http://dx.doi.org/10.3324/haematol.2010.026310>
52. Pizzitola I, Anjos-Afonso F, Rouault-Pierre K, Lassailly F, Tettamanti S, Spinelli O, Biondi A, Biagi E, Bonnet D. Chimeric antigen receptors against CD33/CD123 antigens efficiently target primary acute myeloid leukemia cells in vivo. *Leukemia* 2014; 28:1596-605; PMID:24504024; <http://dx.doi.org/10.1038/leu.2014.62>
53. Schlimper C, Hombach AA, Abken H, Schmidt-Wolf IG. Improved activation toward primary colorectal cancer cells by antigen-specific targeting autologous cytokine-induced killer cells. *Clin Dev Immunol* 2012; 2012:238924; PMID:22481963; <http://dx.doi.org/10.1155/2012/238924>
54. Tettamanti S, Marin V, Pizzitola I, Magnani CF, Giordano Attianese GM, Cribioli E, Maltese F, Galimberti S, Lopez AF, Biondi A, et al. Targeting of acute myeloid leukaemia by cytokine-induced killer cells redirected with a novel CD123-specific chimeric antigen receptor. *Br J Haematol* 2013; 161:389-401; PMID:23432359; <http://dx.doi.org/10.1111/bjh.12282>
55. Chan JK, Hamilton CA, Cheung MK, Karimi M, Baker J, Gall JM, Schulz S, Thorne SH, Teng NN, Contag CH, et al. Enhanced killing of primary ovarian cancer by retargeting autologous cytokine-induced killer cells with bispecific antibodies: a preclinical study. *Clin Cancer Res* 2006; 12:1859-67; PMID:16551871; <http://dx.doi.org/10.1158/1078-0432.CCR-05-2019>
56. Huang J, Li C, Wang Y, Lv H, Guo Y, Dai H, Wicha MS, Chang AE, Li Q. Cytokine-induced killer (CIK) cells bound with anti-CD3/anti-CD133 bispecific antibodies target CD133(high) cancer stem cells in vitro and in vivo. *Clin Immunol* 2013; 149:156-68; PMID:23994769; <http://dx.doi.org/10.1016/j.clim.2013.07.006>
57. Kaneko T, Fusauchi Y, Kakui Y, Masuda M, Akahoshi M, Teramura M, Motoji T, Okumura K, Mizoguchi H, Oshimi K. A bispecific antibody enhances cytokine-induced killer-mediated cytolysis of autologous acute myeloid leukemia cells. *Blood* 1993; 81:1333-41; PMID:8095165
58. Tita-Nwa F, Moldenhauer G, Herbst M, Kleist C, Ho AD, Kornacker M. Cytokine-induced killer cells targeted by the novel bispecific antibody CD19xCD5 (HD37xT5.16) efficiently lyse B-lymphoma cells. *Cancer Immunol Immunother* 2007; 56:1911-20; PMID:17487487; <http://dx.doi.org/10.1007/s00262-007-0333-0>
59. Zhang L, Hou Y, Zhang J, Hu J, Zhang K. Cytotoxicity of cytokine-induced killer cells targeted by a bispecific antibody to gastric cancer cells. *Oncol Lett* 2013; 5:1826-32; PMID:23833649
60. Lu J, He ML, Wang L, Chen Y, Liu X, Dong Q, Chen YC, Peng Y, Yao KT, Kung HF, et al. MiR-26a inhibits cell growth and tumorigenesis of nasopharyngeal carcinoma through repression of EZH2. *Cancer Res* 2011; 71:225-33; PMID:21199804; <http://dx.doi.org/10.1158/0008-5472.CAN-10-1850>